Journal of Chemical Health Risks
www.jchr.org
JCHR (2025) 15(4), 391-408 | ISSN:2251-6727

Pyridine-Derived Chelates: Synthesis, Characterization, Antimicrobial screening and their Potential as Anti- H. Pylori, Antibreast Cancer and Anti-COVID-19 Agents

Tahani Younis Aeyad[1], Adel Mohammed Elbehery[2]and Ibrahim Fouad Mohamed[3]*

[1]Department of Chemistry, , Faculty of science, Almarj, Benghazi University, Libya

[2]Chemistry Department, school of basic science, Libyan Academy - Ajdabiya, Libya

[3] Biochemistry Department, Faculty of Medicine, Almarj, Benghazi University, Libya

***Corresponding author:** Ibrahim Fouad,

(Received: 27 February 2025 Revised: 05 March 2025 Accepted: 18 April 2025)

KEYWORDS

Schiff base; Anti-COVID-19; H-Pylori; DFT; antimicrobial activity; anticancer activity; spectral studies

ABSTRACT:

The metal complexes of a novel pyridine-derived Schiff base ligand. 2-((pyridin-2-ylmethylene)amino)phenol (HL) was investigated. The resultant complexes were identified by elemental analysis, molar conductivity and spectral techniques. Thermogravimetry (TG/DTG) examination further confirmed the presence of water molecules in all studied complexes.Chemical properties of the compounds, such as chemical hardness, dipole moments and HOMO-LUMO energy gaps, were studied using Density Functional Theory (DFT). The computation indicated that the preferred geometry of the complexes was a distorted octahedral structure.

Biological activity of the synthesized compounds was evaluated. They possessed broad-spectrum antimicrobial activities against a selection of bacteria, yeasts and fungi tested, with the Zn(II) complex as the most effective. The complexes also stopped MCF-7 cells (breast carcinoma) from growing into cancer. Their anticancer activity was strongest. In addition, the test shows that these compounds' toxicity toward normal VERO cells is lower than cisplatin. Molecular docking based on DFT was used to study how the compounds interact with several protein receptors splice on their C-terminal tail, with particular attention paid to their inhibitability by H. Pylori, Tumor, and COVID-19.

Introduction

Schiff base complexes derived from pyridines are attracting a great deal of interest as their biomedical applications have been reported [1]. Recent developments encourage the exploration of these unique complexes for their advantageous fusion of chemistry and coordination characteristics, especially in combination with transition metals [2]. Due to their diverse biological activities such as antimicrobial, antifungal, and anticancer properties [3-7], Schiff bases are widely known. It has been shown in several investigations that they play a key role as transport mechanisms for multiple bioactive agents. Spectroscopic and crystallographic characterization of the chemical structure of these compounds is an essential part of the research surrounding them.

Despite the many drugs that can be found on the market, the search for a new drug, with a better mechanism of action and low toxicity in man continues to be one of the major problems for the medicinal chemist. While Schiff bases, their derived complexes and their broad scope of biological activities and diseases have been studied by some researchers, work on the biological activities of the pyridine Schiff bases and their M(II) complexes have begun to be explored. The invention of new types of anticancer agents, which effectively kill cancer cells with low side effects, is intractable [7-10]. Introduction Schiff base complexes have emerged from its class of compounds due to its diverse pharmacological activities of high profile for its anticancer potential [10– 15]. These activities depend on both the nature of metal ions and ligation. Pyridine-derived Schiff base complexes have interesting interactions with various biologically relevant targets, which is essential for the targeted transport of drug molecules to their target sites. The interaction of these complexes with proteins and enzymes is likely to strongly modulate biological activity through intrinsic pharmacological mechanisms. Examining these

Journal of Chemical Health Risks
www.jchr.org
JCHR (2025) 15(4), 391-408 | ISSN:2251-6727

interactions in aqueous solutions provides valuable information about complex stability and implications for potential application before in vivo experiments can be designed.

This study intends to synthesize a new Schiff base via the condensation of 2-pyridine carbaldehyde and 2-aminophenol. The present work plans to develop new complexes based on this new Schiff base with first row transition metals. Various physico-chemical techniques are utilized to comprehensively characterize the synthesized compounds. Assesment of the Biological Activities of a Schiff base and its Metal complexes as Antibacterial, Antifungal and Anticancer Potentials were studied. Taken together, molecular docking studies elucidated the possible binding modes of the ligand and extends of its Zn (II) complex at the active sites of different receptors. This study was intended to characterize some of their chemical and biological properties and to discuss their putative medicinal applications.

2. Experimental section

2.1. Chemicals and reagents.

Chemical precursors from Sigma-Aldrich The chemicals used were of grade AR (99.99%) only. All experimental procedures were always performed using bidistilled water (Brazzini Lopes et al., 2014). MCF-7 human tumor cell lineThe MCF-7 tumor cell line was purchased from the American Type Culture Collection, -180 °C and kept according to the sequential sub-culturing method for checking its viability and continuous proliferation.

2.1. Instrumentation

Characterization of synthesized complexes using different analytical techniques. The carbon, hydrogen, and nitrogen contents were determined by elemental analysis (CHN) (CHNS-932, Cairo University). Triforce XMTD-3000 was used for melting point determination. Metals were analyzed by inductively coupled plasma atomic absorption spectrometry (ICP-AAS). The Fourier transform infrared (FT-IR) spectroscopic analysis was performed in the range of 4000–400 cm−1 by using KBr pellets on a PerkinElmer 1650 spectrometer. Using a Jenway 4010 conductivity meter, the molar conductivity of complex solutions in 10^-3 M of in dimethylformamide (DMF) was obtained. ^{1}H NMR spectra were recorded in DMSO-d6 (tetramethylsilane as internal standard) on a 300 MHz Varian-Oxford Mercury at r.t. An MS-5988 instrument was used for mass spectrometry with electron ionization at 70 eV. Thermogravimetric analysis (TGA/DTG) was performed at room temperature to 1000°C using a Shimadzu TG-50H analyzer. UV-Vis spectrophotometry (200–700 nm) was performed on a PerkinElmer Lambda 20 spectrometer.

2.2. Synthesis of the Schiff base ligand (HL)

HL was prepared by refluxing a mixture of 2-amino phenol (18.32 mmol, 2 g) with 2-pyridine carbaldehyde (18.32 mmol, 1.74 mL) in ethanol. This was then refluxed for 4 hours, between 70 and 100 °C to produce a brown solid. The compound was filtered, recrystallized, washed with diethyl ether and dried under vacuum. In Scheme (1), we show the outline of the structure of HL , and the reactions to obtain it. HL, gave a brown solid, yield 90%, mp 165 °C, with an elemental analysis corresponding closely to the calculated values for C12H10N2O.

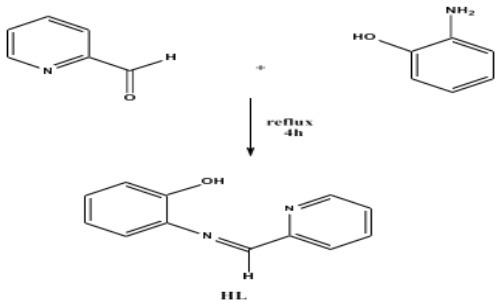

Scheme. 1. Synthesis pathway of the Schiff base ligand (**HL**).

2.3. Preparation of metal complexes

A hot ethanolic solution (60 °C) of a 1:1 molar ratio of the metal chlorides (1.19 mmol) and HL (0.4 g, 2.02 mmol) were reacted to afford metal complexes. The mixture was refluxed for 1 h and then the complexes precipitated out. The powders collected by filtration were then subjected to purification by washing several times with diethyl ether.

2.4. Computational methodology

The DMOL3 program embedded in the Materials Studio was used to perform all density functional theory (DFT) calculations. This approach does full DFT in large-scale double numerical plus polarization (DNP) basis sets that are a more accurate equivalent to respective Gaussian basis sets of the same size [16-22]. Geometries of the unprotonated states were optimized in the GGA-RPBE

Journal of Chemical Health Risks
www.jchr.org
JCHR (2025) 15(4), 391-408 | ISSN:2251-6727

functional that has performed well in correlation. Essential quantum chemical parameters were calculated. These were calculated to give the electronic properties and hence the chemical reactivity of the ligand and complexes.

2.5.Biological in Vitro Studies

Antimicrobial activity Studies

The solution (at concentration of 10 mg/mL, 20 mL was added to the flask), was filtered through a 5 mm filter paper disk. All flasks were autoclaved at 121°C for 20 minutes. Then, four bacterial types, including two Gram-positive (*Staphylococcus aureus, Streptococcus mutans*) and three Gram-negative (*Escherichia coli, Klebsiella pneumonia, Pseudomonas aeruginosa*), and one fungus (*Candida albicans*) were applied and spread on LB agar media surfaces by using the diffusion agar method [17]. Placement of a defined amount of saturated disk, saturated with a solution to be tested, in the middle of the Petri way (agar plates) Twenty two compounds were tested: four (i.e., two copies in every 3 by 2 dimensional arrangement) Petriplates (inoculated before the experiment with strain LHC to others) were placed at equal 2-cm distance from the center of the compounds to be tested. DMSO was used as a control. After these skip executions, the samples were maintained in Petri dishes where they remained at 25°C (1 of these at a time), for 2 more days until the clear, or inhibition, zones around each disk were seen and measured. Each microorganism was placed in a control flask based on the above experimental conditions, thereby creating a baseline for comparison. Here, the application was specific to the solution with DMF. In each experimental case, the diameter of inhibition zone formed due to dimethylformamide was deducted for calculating the antibacterial activity [18, 19]. Amikacin was used as external standard and Ketoconazole as external standard for antibacterial and antifungal activity respectively. Data are means ±, n = triplicate experiments

2.4.1. **Resolution of anticancer assays**

Cytotoxicity In vitro Assay: MTT Method

Using the MCF-7 human breast cancer cell line, the in vitro cytotoxicity of newly compounds was tested[14], [15]. Of the synthesized compounds using the MTT assay to test cytotoxicity, and within the manufacturer's recommendations and instructions. MCF-7 cells in 100 µl of growth medium were plated at 5 × 10^3 cells/well in a clear, flat-bottomed 96-well plate. After attachment for 24 h the number of surviving cells can be counted. The dilution method is a modification of the method which is applied in clinical pharmacology experiments where large numbers of compounds need testing and hence more even distributions are required. In order to concentrate them like stock solutions, the compounds were dissolved in phosphate-buffered saline (PBS, pH~7.4). In growth medium (2-16) or the growth medium containing the diluted compounds(50-400µM) to remove spent growth medium, cells were treated with these from spent growth mediums for 24 hours at 37.5 degrees

C. To serve as controls in this experiment, the same conditions under which the mixed solvent (PBS) was added were applied to posterior aspects of the compound-testing dishes. As a control, cisplatin was used. After 24 hours of incubation, the MTT labelling reagent was added to each well for 10 µl (final concentration (0.5 mg/ml)) and incubated for 4 hours at 37.5°C under an atmosphere of 5% CO2 by volume and with a great many halogen lamps for lighting all around. The pure MTT in no dimethylsulfoxide at all solubilized DMSO, and a final optical density of each well measured at 570 nm using the Multiskan™ FC Microplate photometer (Thermo Fisher Scientific). There were 3 independent replications, each with different cell cultures.

2.5.3. Molecular docking

Molecular docking-based rigid Interaction analysis in Materials Studio Software Suite A well-established in silico tools were employed for the rigid molecular docking analysis. These analyses enable to predict possible binding modes of (HL) and its complexes towards relevant receptors. Crystal structures of major receptors (2JFZ, 1SC7, and 6W41) (for details, see Fig. 3). These functions included the calculation and visualization of potential docked poses of receptors with the Schiff base ligand (HL) and its stable metal complexes. The software takes input of (HL), its corresponding, co-crystallized ligands, and unsupported elements (Na, K, and Hg), were deleted, whereas amino acid chains were retained for analysis [21]. HL and its complexes were designed in the Material Studio software package and saved with PDB file. Crystal structures for different receptors were obtained from the Protein Data Bank. This enabled the preliminary investigations of binding interactions and the correlation of HL and its associated complexes to major receptors to facilitate their therapeutic usages.

Journal of Chemical Health Risks
www.jchr.org
JCHR (2025) 15(4), 391-408 | ISSN:2251-6727

RESULTS AND DISCUSSION

3.1. Pydridine based HL characterization

The elemental analysis results of the synthesized ligand (HL (2-((pyridine-2-ylmethylene)amino)phenol) were in good conformance with the calculated values for C, H and N. It matches with the proposed formula with the chemical formula identical to ligand C12H10N2O9 (Fig.1). HL was obtained as a stable brown solid at room temperature and soluble in ethanol and DMF.

The mass spectrum of HL presented a molecular formula with a molecular ion peak appearing at m/z 197 amu (C12H10N2O atomic weight = 198 amu). Relative Peaks for the Individual Components of the Ligand Was Also Observed. For HL, the 1H NMR spectra were found to show multiplet signals in the range of 6.25–6.88 ppm, which were due to aromatic ring protons [22]. The signals at 10.48 ppm and 8.70 ppm were ascribed to the OH group and azomethine proton [23].

In IR spectra of parent ligand, azomethine group CH=N formed as a result of condensation was detected with an intensive band at 1593 cm-1 [24]. This corresponded with the comparable peak found at 1655 cm− in the DFT study [18]. The successful synthesis of Schiff base ligand is confirmed by the good correlation between experimentally observed and theoretically calculated frequency [18]. Systematic errors inherent in the harmonic approximation or related to DFT calculations being performed on gas-phase molecules [25, 26] could lead to discrepancies that are apparent between theoretical and experimental frequencies.

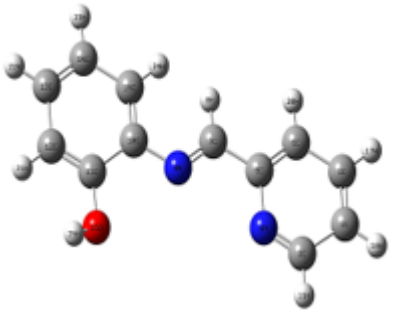

FIGURE. 1. The optimized structure of Schiff base ligand **(HL)**

3.2. Characterization of the Schiff base metal complexes

3.2.1. Elemental analysis

Metal complexes were prepared from the reaction of metal ions with HL in a ratio of 1:1 (metal: ligand) in good yields. The solubility of these metal complexes in various organic solvents such as ethanol, dimethylformamide (DMF) and dimethyl sulfoxide (DMSO) are investigated. Detailed results and data presentation are shown in Table 1. Consequently, this would result in a complex of stoichiometry M: L.

Compound (chemical formula)	Color	M_{P_t} (°C)	Found (Calcd)				μ_{eff}	
			C (%)	H (%)	N (%)	M (%)	(B.M.)	Λ_m (Ω^{-1} mol^{-1} cm^2)
Schiff base ligand (HL)	brown 90%	165	73.84 (73.92)	5.03 (5.08)	13.13 (13.23)	……	……	……
[Cr (L) $(H_2O)_2$ Cl]Cl.$2H_2O$	Reddish brown 84%	100	40.39 (40.88)	4.75 (5.05)	7.02 (7.05	14.50 (14.33)	4.32	65
[Mn (L) $(H_2O)_2$ Cl].$3H_2O$	Brown 83%	105	38.02 (38.23)	4.75 (4.88)	6.80 (6.89	14.50 (14.29)	5.90	42
[Fe (L) (H_2O) Cl_2].$2H_2O$	Brown 83%	180	37.50 (37.64)	3.90 (4.02)	6.88 (6.94)	14.75 (14.99)	5.14	42
[Co (L) $(H_2O)_2$ Cl]	Yellow 85%	›300	44.24 (44.49)	4.92 (5.00)	7.98 (8.10)	18.10 (17.95)	4.98	22
[Ni (L) $(H_2O)_2$]Cl.H_2O	Reddish brown 87%	›300	37.65 (37.85)	4.80 (4.86)	6.79 (6.89)	15.34 (15.68)	3.65	81

Journal of Chemical Health Risks
www.jchr.org
JCHR (2025) 15(4), 391-408 | ISSN:2251-6727

[Cu (L) H_2O)$_3$]Cl.$2H_2O$	Brown 77%	138	36.70 (36.76)	4.55 (4.62)	6.58 (6.60)	16.95 (16.83)	1.70	68
[Zn (L) $(H_2O)_2$ Cl].$2H_2O$	Reddish brown 88%		39.12 (39.65)	4.37 (4.45)	7.05 (7.56	17.71 (17.90)	Diam	25
[Cd (L) $(H_2O)_2$ Cl].$2H_2O$	Brown 87%		34.60 (34.67)	4.09 (4.21)	6.26 (6.43)	27.07 (26.98)	Diam	8

Table 1. Analytical and physical data of Schiff base ligand **(HL)** and its metal complexes.

Yield (%)

3.2.2. Measurements of Molar Conductivity

Where Λm stands for the molar conductance of the complexes and K is the conductance of the metal complex solutions in (C). The ligand (HL) acts as a tridentate anionic ligand with a negative charge. The chelates were solubalised with ethanol and the molar conductivities of 10−3 M solutions at 25 ± 2 °C were measured as previously described. The observed molar conductivities of Ni(II), Cu(II) and Cr(III) chelates (65 and 81 Ω^{-1} mol^{-1} cm^2) indicate that they behave as 1:1 electrolytes (Table 1). On the other hand molar conductance of Co(II), Zn(II), Cd(II), Mn(II), and Fe(III) chelates in the range of 8–42 Ω^{-1} mol^{-1} cm^2 (Table 1) indicates that these chelates are non-electrolyte. 27

3.2.3. FT-IR Spectroscopic Investigations

A detailed comparison of the IR spectra of the complexes in table 2, versus those of the free ligand, allows us to determine whether or not coordination has taken place at the site of chelation. The IR spectra of the ligand (HL) shows a band at 1593 cm–1, which is characteristic of the azomethine ν(C=N) group [29]. In the case of all complexes, the absorption band was much more pronounced and was found in the range of 1626–1653 cm–1, in comparison with the free ligand indicating the involvement of azomethine nitrogen in interaction with the metal ions. In the case of the complexes, the νstr(OH) spectra of the complexes showed broad bands within the 3402–3434 cm–1 range. This is attributed to its organized water molecules [30]. The IR spectrum of the ligand (HL) has a characteristic band at 1476 cm-1,another band can be attributed to the py rridine ν(C=N) group. This band shifts to 1456–1603 cm–1 using complexation [29]. Such change represents the nitrogen availability for coordination with metal ions from the pyridine group [31]. In detail, all of the complexes afforded new bands in the region of 528–552 cm−1, attributed to the ν(M-O) vibrational mode, and at 438–467 cm−1 correlated to the ν(M–N) vibrational mode [32–36]. The ligand (HL) features uninegative tridentate chelation, representing three chelating sites attached to the metal ion [one nitrogen from the pyridine moiety, one phenolic oxygen, and one azomethine nitrogen atom from the Schiff base]. All of these are octahedral complexes in which, respectively, three molecules of water are coordinated and two molecules of water and one atom of chloride.

Table 2. The most significant infrared (IR) spectral bands of the isolated Schiff base ligand (HL) ternary Complexes are as follows:

Compound	υ [OH]	υ [C=N]	υ [C=N] pyridine	H_2O stretching of coordinated water	υ [M-O]	υ [M-N]
Schiff base ligand (HL)	**3420 sh**	**1593 sh**	**1476 m**			
[Cr (L) $(H_2O)_2$ Cl]Cl.$2H_2O$	**3420 sh**	**1648 sh**	**1456 m**	**920 w, 870 w**	**556 w**	**443 w**
[Mn (L) $(H_2O)_2$ Cl].$3H_2O$	**3402 sh**	**1651 w**	**1590 w**	**915 w, 866 w**	**590 w**	**462 w**
[Fe (L) (H_2O) Cl_2].$2H_2O$	**3418 br**	**1644 sh**	**1587 w**	**920 w, 845 w**	**555 w**	**438 w**

Journal of Chemical Health Risks
www.jchr.org
JCHR (2025) 15(4), 391-408 | ISSN:2251-6727

[Co (L) (H2O)2 Cl]	**3404 sh**	**1649 sh**	**1587 sh**	**925 w, 860 w**	**550 w**	**440 w**
[Ni (L) (H2O)3]Cl.H2O	**3404 br**	**1626 m**	**1467 sh**	**910 w, 855 w**	**536 w**	**466 w**
[Cu (L) (H2O)3]Cl.2H2O	**3441 sh**	**1629 w**	**1596 w**	**900 w, 845 w**	**528 w**	**459 w**
[Zn (L) (H2O)2 Cl].2H2O	**3434 br**	**1653 sh**	**1603 w**	**925 w, 878 w**	**546 w**	**467 w**
[Cd (L) (H2O)2 Cl].2H2O	**3423 br**	**1652 m**	**1595 w**	**900 w, 850 w**	**552 sh**	**463 w**

Sh=sharp, br=broad, w=weak.

3.2.4. ^{1}H NMR spectral studies

The 1H NMR spectra of Schiff base ligand and corresponding Zn(II) and Cd(II) complexes are recorded at DMSO-d6 with tetramethylsilane (TMS) as internal standards [25], [28] and listed in Table [3]. The protons of aromatic ring of 2-amino phenol displayed as multiplets in the peaks range of (6.25 - 6.88), (6.30 - 6.84), and (6.15 - 6.64) ppm for the ligands HL, and respectively complexes [Zn(L)(H2O)2Cl]·2H2O and [Cd(L)(H2O)2Cl]·2H2O [37]. Multiplets for the aromatic protons also appeared in the 1H NMR spectra for the pyridine ring of the free HL ligand as well as the [Zn(L)(H2O)2Cl]·2H2O and [Cd(L)(H2O)2Cl]·2H2O complexes (7.17 - 8.85), (7.09 - 8.80) and (7.02 - 8.82) ppm, respectively [37]. For the HL ligand, [Zn(L)(H2O)2Cl], a singlet band belonging to the azomethine group was detected at 8.70, 8.66 and 8.72 ppm. 2H2O, and [Cd(L)(H2O)2Cl]. The OH signal is missing from the spectra of [Zn (L) (H2O)2 Cl]. 2H2O and [Cd(L)(H2O)2Cl]. The presence of the 2H2O complexes indicated that the HL ligand acts as a uninegative ligand which was found to be due to deprotonation of the ligand during complexation as opposed to the free shiff base(9.48 ppm)[37,38].

Table 3. ^{1}H NMR spectral data of HL and its Zn and Cd metal chelates.

Compound	Chemical shift, (δ) ppm	Assignment
(HL)	**9.48**	**(s, 1H, OH)**
	6.25 - 6.88	**(m, 4H, ArH 2-amino phenol)**
	7.17-8.85	**(m, 4H, pyridine ring)**
	8.7	**(s, 1H, azomethine)**
[Zn (L) (H2O)2 Cl].2H2O	**Disappear**	**(s, H, OH)**
	6.30-6.84	**(m, 4H, ArH 2-amino phenol)**
	7.09-8.80	**(m, 4H, pyridine ring)**
	8.66	**(s, H, azomethine)**
[Cd (L) (H2O)2 Cl].2H2O	**Disappear**	**(s, H, OH)**
	6.15-6.64	**(m, 4H, ArH 2-amino phenol)**
	7.02-8.82	**(m, 4H, pyridine ring)**
	8.72	**(s, H, azomethine)**

Journal of Chemical Health Risks
www.jchr.org
JCHR (2025) 15(4), 391-408 | ISSN:2251-6727

3.2.5. Ultraviolet-Visible Spectral investigation

The UV-Vis spectra of ligand HL and its complexes were registered at ambient environment with a UV-Vis spectrophotometer. The UV-visible spectrum of HL has a strong band at 237 nm which most plausibly originates from a π → π* transition of the aromatic rings. An absorption band is also observed at 388 nm, which is most likely due to the n→π transition of azomethine. This was followed by a bathochromic shift of the bands at 264– 272 and 292– 294 nm for π→π and n→π* respectively, after UV–Vis spectrum investigation for the bonding of azomethine nitrogen to the metal centers [39]. One of the most important electronic transitions were the d-d transitions for the Co(II) complex, which were characterized in the UV-Vis spectra by visible bands with distinct wavelengths (653 nm).

3.2.6. Thermogravimetric analysis (TG and DTG) of HL Ligand and its metal complexes

HL thermal decomposition was distinguished by four degradation stages (the beginning and end of these stages were 89 °C and 750 °C, respectively). The first two breakdown stages (weight loss was 34.90% (calculated was 34.51%)) occurring between 35–335 °C corresponded to loss of H2O and C4H4. Third and fourth decomposition processes happen in the temperature region of 335-1000 °C and C8H6N2 molecule is lost; the total weight loss is up to 65.00% (theoretical calculation: 64.49%) and so the total loss is reach 99.9% (99%) [33].

Thermal gravimetric analysis (TG) [40] was utilized to explore attempts in coordinated associated water or solvent molecules about the coordination sphere or in the crystalline phase. Table 4 holds information that we have obtained from gravimetric analysis (TG) of the complexes (at 25 °C to 800 °C in a nitrogen atmosphere) and it shows the different stages of decomposition with corresponding temperature regions, and weight losses percentage of the compounds.

08652 and 08645) and determined the breakdown steps from the TG curve of [Cr(L)(H2O)2Cl]Cl·2H2O complex. In the temperature range of 40–340 °C, H2O, Cl2, and C2H2 molecules were removed in stages 1 and 2, providing a mass loss of 46.80% (the theoretical value for the loss was 47.20%). The degradation process in stage 3 involves the release of C3H2N molecules in the temperature range of 340–580 °C, producing a mass loss of 14.27% (calculation figure is 14.07%). The initiation of the fourth and sixth stages, which occurred in the temperature ranges of 580–1000 °C, is associated with the removal of C7H5N molecules, contributing to a mass loss of 29.30% (29.70% estimated). After taking into account 90.97% (estimated as 91.17%) of the total weight loss, only chromium oxide containing carbon atoms remains [27].

TG analysis results for [Mn(L)(H2O) 2 Cl]. Decomposition of the 3H2Ocompound proceeds in four stages. In the first step, a loss of 15.10% (est. 15.49%) by weight occurs over the temperature range of 35–120 °C due to the release of three water molecules (3H2O). In the next stage, the 2H2O is released, leading to 9.40% of weight loss (9.27% estimated) at 120–240 °C. Stage III, occurring between 240 and 815 °C, similarly accounts for the loss of ½Cl2 plus a C5H4N molecule (29.07 wt% loss measured, 29.70 wt% estimated). Step four (815–1000 °C): Loss of one C3H5N (weight loss of 13.00% (measured) vs. 12.73% (calculated)). The last step corresponds to the elimination. C[O.sub.3]nd the final stage residue of calcination is MnO. 2])[12] with a mass loss of 66.23% in total (calculated at 66.36%) while having a residue still contains carbon atoms.

In these curves are similar to the TG curve of [Fe (L)(H2O)Cl2]. 2H2O dissociates, and the same happens in a four-stage process, in reverse. The temperature from 35–170 °C is the first stage, where the loss of weight 9.4% (estimated at 9.10%) is produced by the elimination of non- coordinated 2H2O molecules. The following steps (170–675 °C) are related to the step-by-step liberation of H2O, Cl2, and C3H3N, with a total mass loss of 37.19% (theoretically 37.50%). Step 4: After 675–1000 °C gives one unit of C9H6N, leading to 30.33% weight loss (in quantity 30.52% weight loss). The system achieved a total weight loss of 76.92% (theoretically 77.12%), and a residue of pure ferric oxide is obtained.

The decomposition steps of the [Co(L)(H2O)2Cl] complex are sequentially shown in the thermogravimetric analysis of FIGURE 5. The first two stages in the range of 40–340°C are ascribed to the liberation of 2H2O and ½Cl2 molecule, confirming a total weight lost of 19·50% (calculated at 19·17%). The last breakdown step releases the C6H5N molecule with 30.05% (calculated at 30.10% too) weight loss in the temperature interval of 340–685°C. In the following fourth and sixth stages step during the temperature of 685–1000°C, it could remove the C3H4N species (weight loss: 17.60% estimated weight loss: 17.97%).

Journal of Chemical Health Risks
www.jchr.org
JCHR (2025) 15(4), 391-408 | ISSN:2251-6727

The total mass loss is (66.72% summarized as 66.21%) leading to cobalt oxide remains in the presence of carbon atoms.

Likewise, the TG thermogram of [Ni(L)(H2O)2Cl]. Cl. This means that the decomposition takes place in five steps. In stage I (35–100 °C), the 3H2O molecules coordinated to the framework are liberated leading to a weight loss of 12.68% (theoretical 12.36%). Mean mass losses due to the removal of coordinated 2H2O molecule (100–210 °C, 9.00% weight loss, calculated 8.69%), ½Cl2 (210–310 °C, 8.88% weight loss, calculated 8.44%), and C9H9N2 molecule (310–1000 °C, 36.90% weight loss, calculated 37.02%) are derived from the following stages of the respective TGA thermograms. Then followed with a carbonization of the nickel oxide residues, resulting in an overall weight reduction of 67.46% (theoretical 66.53%).

An example of this is the thermogravimetric analysis of [Cu(L)H2O)3] (figure [9] Cl. Thermodynamic Analysis The breakdown of the 2H2O complex is divided into five phases. A mass loss of 49.30% (calculated as 49.71%) occurred within the first three steps at between 35 and 615°C, corresponding to the loss of 5H2O, ½Cl2, and C4H4N molecules, respectively. Stage two involves the removal of the coordinated C5H6N molecule, which occurs at 615-1000°C, with a corresponding mass loss of 19.40% (theoretical mass loss 19.89%). of the whole loss of weight is 68.70% (based value is 69.63%), and then the ash residue is black copper oxide with carbon atoms.

Thermogravimetric (TG) analysis of [Zn(L)(H2O)2Cl]. The breakdown of the 2H2O complex seems to occur through three phases. The first two steps (35–320 °C) correspond to the loss of 4H2O and ½Cl2 molecules, leading to 33.70% (calculated 33.50%) of weight loss from the respective chlorohydrate product. Third stage of the decomposition between 320 and 1000 °C, with leaving coordinated C12H9N2 molecule and the losing weight is 52.08% (calculated is 51.67%). The sum of the masses that lost (85.78% — theoretical: 85.17%) gives us the mass of zinc oxide.

TG analysis of [Cd(L)(H2O)2Cl] in 3. The 2H2O complex is processed through four breakdown stages. The first step, which occurs at a temperature of 35–210 °C, is associated with the removal of 2H2O molecules that are not connected, with weight loss of 8.40% (calculated of 8.10%). In the next stage, a mixture of char−2H2O and ½Cl2 was removed in the temperature range of 210−345 °C, leading to a weight loss of 15.22% (theoretical 15.15%). Degradation in the range of 345–1000 °C (i.e., third and fourth breakdown phases) corresponds well to the loss of C12H9N2 (calculated 44.86%, observed 45.28%). During this case, the sum loss of weight is 67.90%(as total 68.11%)[13] and the by-product is cadmium oxide.

Table 4. Thermoanalytical results (TG and DTG) of HL and its metal complexes.

Complex	TG-range (ºC)	DTG max	n*	Mass loss (calcd)% (Total mass Loss)	Estim	Assignment	Residues
$C_{12}H_{10}N_2O$	**35-335**	**89,187**	**2**	**34.90(34.51)**		**-Loss of C_4H_6O**	
	335-1000	**371, 750**	**2**	**65.00(64.49)**		**-Loss of $C_8H_6N_2$**	
				99.9(99)			
[Cr (L) $(H_2O)_2$ Cl]Cl.$2H_2O$	**40-340**	**74,319**	**2**	**46.40(47.20)**		**-loss of 3H2O, Cl2,C2H2**	**½ Cr_2O_3**
	340-580	**575**	**1**	**14.27(14.07)**		**-Loss of C_3H_2N**	
	580-1000	**871,925**	**2**	**27.20(29.70)**		**- Loss of $C_6H_4NO_{0.5}$**	
				87.87(91.17)			
[Mn (L) $(H_2O)_2$ Cl].$3H_2O$	**35-120**	**67**	**1**	**15.10(15.49)**		**-Loss of 3H2O**	

Journal of Chemical Health Risks
www.jchr.org
JCHR (2025) 15(4), 391-408 | ISSN:2251-6727

	120-240	188	1	9.40(9.27)	-Loss of 2H2O	4C+MnO
	240-815	590	1	29.07(29.70)	-loss of ½Cl2,C5H4N	
	815-1000	840	1	13.00(12.73)	-Loss of C3H5N	
				66.23(66.36)		
[Fe(L) (H2O) Cl2].2H2O	35-170	74	1	9.40(9.10)	Loss of 2H2O	½Fe2O3
	170-675	227,515	2	36.40(37.50)	-Loss of Cl2,C4H6N	
	675-1000	820	1	32.18(30.52)	-Loss of C8H5NO0.5	
				77.98(77.12)		
[Co (L) (H2O)2 Cl]	40-340	168,262	2	19.50(19.17)	-Loss of 2H2O, ½Cl2	
	340-685	627	1	30.05(30.10)	-Loss of C6H5N	3C+CoO
	685-1000	772,886	2	17.60(17.97)	-Loss of C3H4N	
				66.72(67.21)		
[Ni (L) (H2O)3]Cl.H2O	35-210	78,198	2	23.06(21.08)	-Loss of 2H2O, ½Cl2	
	210-1000	258, 406, 925	3	46.13(45.46)	-Loss of 2H2O, C6H9N2	
				69.19(66.53)		6C+NiO
[Cu (L) H2O)3]Cl.2H2O	35-615	70,157,220	2	49.30(49.71)	-Loss of 5H2O,	CuO+3C
	615-1000	685	1	19.40(19.89)	-Loss of C5H6N	
				68.70(69.63)		
[Zn (L) (H2O)2 Cl].2H2O	35-320	65,235	2	33.70(33.50)	-Loss of 4H2O, ½Cl2	ZnO
	320-1000	526	1	52.08(51.67)	-Loss of C12H9N2	
				85.78(85.17)		
[Cd (L) (H2O)2 Cl].2H2O	35-210	67	1	8.40(8.10)	-Loss of 2H2O	CdO
	210-345	214	1	15.22(15.15)	-Loss of 2H2O, ½Cl2	
	345-1000	668,890	2	45.28(44.86)	-Loss of C12H9N2	
				67.17(68.11)		

3.2.9. Geometry optimization

DFT method was used to determine the geometry optimization HL and its Zn(II) complex specifically due to its prominent biological activity related to its history [51]. The numbering of each atom is given in table 5 in its caption, and all fully optimized geometries are provided in the following. Bond lengths and angles were calculated and shown in table 6 [52], which shows a distorted octahedral geometry importantly surrounding the Zn(II) ion. Upon coordination through azomethine nitrogen, the azomethine group of pyridine, and the phenolic-O, the bond lengths C(11)–O(16), N(9)–C(10), C(7)–N(9), N(4)–C(5), and C(3)–N(4) in the Zn(II)

Journal of Chemical Health Risks
www.jchr.org
JCHR (2025) 15(4), 391-408 | ISSN:2251-6727

complex were (or were extended) over the ligand (HL) (Table 4) [24.

Global Reactivity Descriptors of the Schiff base ligand (HL) and its Zn(II) complex (Table 6) [53]. Standard computational methods are used to obtain the molecular properties [12]. The energy difference ΔE between highest occupied molecular orbital (HOMO) and lowest unoccupied molecular orbital (LUMO) is calculated as ΔE = ELUMO − EHOMO. That is,(7)Absolute softness(σ) :σ=1/η(8)Excess electron charge(ΔNmax):ΔNmax=−I/η Charge transfer interactions between the molecule, which affect biological activity, lead to a lower energy gap [4]. The activity gap is a crucial element to determine the reactivity of the chemical species for small frontiers orbital gap, indicates more reactive of the molecule, considered as "soft" molecule. It represents an important stability metric taking into account not only structural but also conformational barriers in an array of molecular systems. For the Schiff base ligand (HL) and its Zn (II) complex the values of energy gaps are

2.544 e V and 1.662 e V, respectively. The higher the energy gap, the more stable the compound. Similarly, the chemical potential (Pi) was negative and the electrophilicity index (χ) was positive. This would support the idea that ligand is likely to be an electron donor towards metal ions [54].

Table 5. Molecular Orbital Analysis of HOMO and LUMO for Schiff Base Ligand **(HL)** and its Zn **(II)** Complex Computed Using DFT Methodology.

Optimized geometry visualization of the studied Schiff base (L) and its Zn (II) Complex

Compound	optimized structure	3D-HOMO	3D-LUMO	ΔE (eV)
Schiff base ligand (HL)	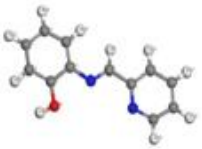	 E_{HOMO} = -4.764eV	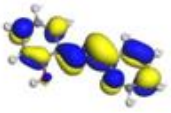 E_{LUMO} = -2.220eV	2.544
$[Zn(L)(H_2O)_2Cl].2H_2O$	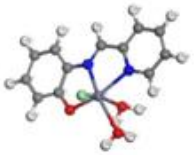	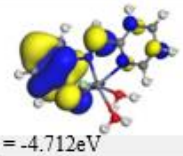 E_{HOMO} = -4.712eV	 E_{LUMO} = -3.050eV	1.662

TABLE. 6. Optimized and Quantum Chemical Parameters for Schiff Base Ligand **(HL)** and Its Zn (II) Complexes: A Comparative Analysis

The calculated quantum chemical parameters	**Schiff base ligand (HL)**	**$[Zn(L)(H_2O)_2Cl].2H_2O$**
Dipole moment (Debye)	**1.9120**	**4.669437**
EHOMO (eV)	**-4.764**	**-4.712**
ELUMO (eV)	**-2.220**	**-3.05**
ΔE (eV)	**2.544**	**1.662**
χ(eV)	**3.492**	**3.881**
η(eV)	**1.272**	**0.831**
$\sigma(eV)^{-1}$	**0.786163522**	**1.203369434**
Pi (eV)	**-3.492**	**-3.881**
S $(eV)^{-1}$	**0.393081761**	**0.601684717**

Journal of Chemical Health Risks
www.jchr.org
JCHR (2025) 15(4), 391-408 | ISSN:2251-6727

ω(eV)	**4.793264151**	**9.062672082**
ΔNmax	**2.745283019**	**4.670276775**
Bond lengths (Å)	**Schiff base ligand (L)**	**[Zn(L)(H2O)2Cl].2H2O**
N(9)-C(10)	**1.404**	**1.382**
C(7)-N(9)	**1.290**	**1.301**
C(11)-O(16)	**1.377**	**1.316**
N(4)-C(5)	**1.356**	**1.369**
C(3)-N(4)	**1.338**	**1.346**
Bond angles (o)	**Schiff base ligand (L)**	**[Zn(L)(H2O)2Cl].2H2O**
O(20)-Zn(17)-Cl(19)	**----------**	**165.915**
O(20)-Zn(17)-O(18)	**----------**	**76.07**
O(20)-Zn(17)-O(16)	**----------**	**80.001**
O(20)-Zn(17)-N(9)	**----------**	**84.141**
O(20)-Zn(17)-N(4)	**----------**	**84.506**
Cl(19)-Zn(17)-O(18)	**----------**	**89.846**
Cl(19)-Zn(17)-O(16)	**----------**	**102.54**
Cl(19)-Zn(17)-N(9)	**----------**	**109.928**
Cl(19)-Zn(17)-N(4)	**----------**	**97.846**
O(18)-Zn(17)-O(16)	**----------**	**98.099**
O(18)-Zn(17)-N(9)	**----------**	**160.114**
O(18)-Zn(17)-N(4)	**----------**	**99.37**
O(16)-Zn(17)-N(9)	**----------**	**80.11**
O(16)-Zn(17)-N(4)	**----------**	**153.073**
N(9)-Zn(17)-N(4)	**----------**	**76.491**

3.3. Biomedical sudies

3.3.1. Antimicrobial properties

It has been reported that chelation is responsible for the higher antibacterial activity of metal complexes over those of non-chelated Schiff base ligands [52]. Metal ions coordinate the Schiff base through the process by polar and non-polar type of metal chelates [55] Developing this hydrophilic and hydrophobic nature is beneficial as it allows these compounds to penetrate inside cells and tissues more readily. Among these effects, the most important is the decrease in metal ion polarity, which is caused by the overlapping of some of the ligand orbitals and the consequent partial sharing of its positive charge with the donor groups. This leads to improved π-electron delocalization in the chelate ring, which in turn promotes greater ease in complex diffusion across lipid membranes [56, 57]. Competitive ligation of the central metal ions of chelators alters their hydrophilic and lipophilic features, increasing their lipid solubility and enabling them to cross the lipid bilayer of biological membranes. The coordinating process changes the lipophilicity, the important contribution to the cellular aspiration. This correlates to the issue that

Journal of Chemical Health Risks
www.jchr.org
JCHR (2025) 15(4), 391-408 | ISSN:2251-6727

complexes of the metal are within the coordination of a free ligand or transition to a fully active intermediate [56, 58]. All antimicrobials have a fundamental promise: kill the intended bacterial target without harming the patient. The antibacterial activity of the Schiff base ligand and its complexes was investigated against several bacterial strains belonging to five different species. In addition, it was tested against the fungal strain C. albicans [60]. The ligand and its complexes were tested for their biological study using the classical antibacterial agent amikacin and the antifungal agent ketoconazole. The complexes show higher biological activity than that of free ligand. The maximal activity was shown by Zn(II) whereas the Fe(III) complex showed minimal; however all were more active than the average. The antifungal effectiveness of all synthesized ligands and metal complexes against pathogenic fungi was examined and the metal complexes displayed a higher potency effect than free ligand.The synthesized Cd(II), Mn, and Ni(II) complexes showed superior antifungal efficiency compared to the standard. The results from these evaluations are summarized in Table 7 and visualized in Figure 3. The bioactivity assessment of the metal(II)/(III) complexes proves the presence of biological activity for HL against almost all tested bacterial species except for E.Coli where Fe(III) complex exhibited no biological activity.

Table. 7. Biological activity of Schiff base ligand (HL) and its metal complexes.

Sample	**Inhibition zone diameter(mm / mg sample)**					
	Gram positive bacteria		**Gram negative bacteria**			***Candida albicans***
	Staphylococcus aureus	***Streptococcus mutans***	***Escherichia coli***	***Klebsiella pneumonia***	***Pseudomonas aeruginosa***	
Control: DMSO	**0**	**0**	**0**	**0**	**0**	**0**
Ligand(HL)	**0**	**12.3**	**0**	**0**	**12.3**	**21.3**
[Cr(L)(H2O)2Cl]Cl.2H2O	**11.3**	**12.3**	**10.6**	**10.6**	**15.3**	**0**
[Mn(L)(H2O)2Cl].3H2O	**20.6**	**12.3**	**12.6**	**27.6**	**14.3**	**28.6**
[Fe(L)(H2O)Cl2].2H2O	**15.3**	**10.3**	**0**	**11.6**	**13.6**	**12.3**
[Co(L)(H2O)2Cl]	**25.3**	**18.3**	**22.6**	**25.6**	**26.3**	**15.3**
[Ni(L)(H2O)3]Cl.H2O	**20.3**	**14.6**	**13.3**	**12.6**	**10.6**	**26.3**
[Cu(L) H2O)3]Cl.2H2O	**25.6**	**17.3**	**10.3**	**14.3**	**14.6**	**0**
[Zn(L)(H2O)2Cl].2H2O	**30.3**	**14.6**	**22.6**	**38.6**	**19.3**	**18.3**
[Cd(L)(H2O)2Cl].2H2O	**27.0**	**22.6**	**29.0**	**23.6**	**11.0**	**24.3**
Amikacin	**9**	**6**	**6**	**7**	**7**	**-------**

Journal of Chemical Health Risks
www.jchr.org
JCHR (2025) 15(4), 391-408 | ISSN:2251-6727

ketokonazole	-------	-------	-------	-------	-------	9

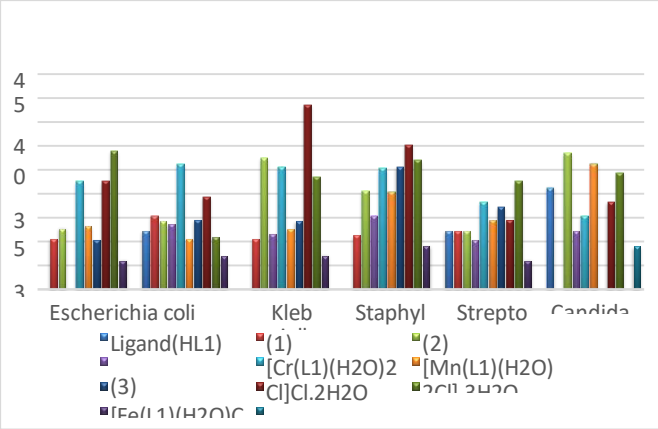

Fig. 3. Assessment of the Bioactivity of HL and its Metal Complexes

3.3.2. Anticancer activities

Identifying new active compounds for cancer treatment is at the forefront of current pharmaceutical research related to the discovery of metal- based antitumor drugs. In this work the study of different transition metal complexes , their synthesis and characterisation have played a crucial role. Laboratory experiments testing the ligand and its complexes for potential cytotoxicity on MCF-7 (breast cancer) cells. Based on the concentration-dependence relationship of the chemicals with the relative cell viability, the survival curves were generated [10] (Fig 4). The values of IC50, i.e., the concentration leading to 50% inhibition of the proliferation of cancer cells are given in Table 8.

All metal complexes of the Schiff base exhibited considerable activity against cancer cell lines, in particular HL. Due to the IC50 values being defined as the concentration of the drug needed to inhibit the growth of 50% cancer cells, these results place these compounds as candidate key anticancer drugs under chemotherapy [24]. Table 8 Comparative evaluation of anticancer activity of uncoordinated Schiff base ligand (HL) and its corresponding metal chelates. The above results indicate that the Zn-complex shows better antitumor activity as compared to the ligand and other metal complexes. While HL showed low cytotoxic activity against the cancer cell line analyzed, the Zn (II) complex showed significant cytotoxic activity, and the Fe (II) complex proved ineffective. Spectacular correlation of anticancer and antimicrobial activities As shown in Table 8, the Zn-complex revealed a very high antifungal and antibacterial effectiveness against all investigated fungal and bacterial species, apart from promising anticancer activity against MCF-7 (breast carcinoma) cells[66].

The intricate compound [Zn(L)(H2O)2Cl]. This is the active and efficient compound 2H2O in this regard and it may play a role in breast cancer as its anticancer agent. The higher activity of the compounds obtained could be explained by the azomethine group (− C = N−) included in the macrocyclic chelate ring. This decrease in polarity is explained by the interaction of the metal ion with the nitrogen of the azomethine group in the chelate ring, which can generate a partial positive charge that is shared with the ligand [62–64]. The opening of the ring on complexation might increase activity as it may lead to higher π−electron delocalisation within the ligand as well as increased lipid bilayer permeability thus increasing penetration of the complexes into the cellular membranes and improving their efficacy [65].

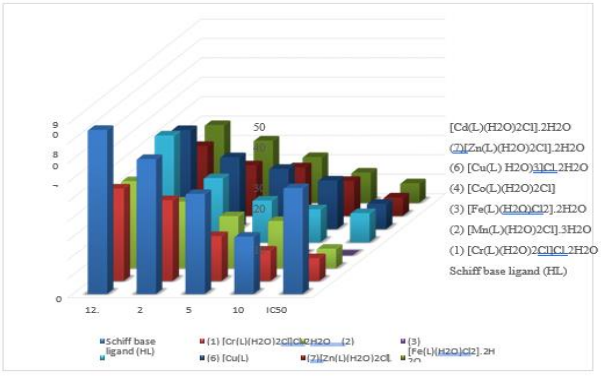

Fig.4. Anticancer activity of HL and its metal complexes

Journal of Chemical Health Risks
www.jchr.org
JCHR (2025) 15(4), 391-408 | ISSN:2251-6727

TABLE 8: Anticancer activity of HL and its metal complexes

Concentration (µg/mL) sample Surviving fraction (MCF-7)	12.5	25	50	100	IC50 (µg/mL)
Schiff base ligand (L)	85	70	52	30	55
[Cr(L)(H2O)2Cl]Cl.2H2O	48	42	23.5	16	12
[Mn(L)(H2O)2Cl].3H2O	45	34.5	27	24.5	10.2
[Fe(L)(H2O)Cl2].2H2O	-	-	-	-	-
[Co(L)(H2O)2Cl]	55	33	21.5	17	15
[Ni(L)(H2O)3]Cl.H2O	72	57	45	32	29
[Cu(L) H2O)3]Cl.2H2O	51	37	31	25	13
[Zn(L)(H2O)2Cl].2H2O	36	26	25	18	9.5
[Cd(L)(H2O)2Cl].2H2O	40	32	23.5	15.5	10

3. Docking study of HL and its zinc complex.

Three different receptors have been studied for exploration of their binding sites for HL and its Zn(II) complex respectively. Table 11 The 2D and 3D plots of the docking results of the Schiff base ligand (HL) and the Zn(II) complex. Tables 9, and 10 show the binding energies for the Schiff base ligand (HL) and its corresponding Zn(II) complex, respectively. The IC50 for the breast cancer cell line was of 55 µg/ml for HL demonstrating that effect in vitro. The Zinc (II) complex showed improved anticancer effect with an IC50 of 9.5 µg/ml [8]. The results are generated according to docking studies achieved on receptors of Human DNA Topoisomerase I (70 kDa) with the indenoisoquinoline MJ-II-38 and a covalent complex with a 22 base pair DNA duplex (PDB ID: 1SC7). Topoisomerase I (top1) A well-known molecular target of different anticancer agents directed against human topoisomerase I (top1) acts by interfering with the enzyme and forming drug-enzyme covalent complexes, Molecular docking analysis of the prepared Schiff base ligand (HL) and its Zinc (II) complex was performed. Conclusion In this work we explored the most stable molecular bond formers with binding energies of -2.5 and -17.4 kcal mol−1. This indicates greater mobility of the complexes compared to that of parent ligand due to the formation of coordination bond between the attractive Zinc (II) metal ion and corresponding donor atom of the ligand. Table [9,10] summarizes the effective and significant interactions of these compounds with different protein receptors of H. pylori and the receptor of SARS-CoV-2. Almost all of the interactions that were observed in a bulkphase were H-donor, H-acceptor, ionic, and π-H interaction forces.

The binding energies (ΔG) of HL and Zn(II) complex are listed in Table 1 for receptors 2JFZ and 6W41 respectively. For the free Schiff base ligand L, the values of NA and −0.7 kcal mol−1 were determined, while values of -4.4 and -12.7 kcal mol−1 were established for the corresponding Zn(II) complex, in particular.

For H. pylori, previously discussed the Schiff base ligand is inactive toward the 2JFZ receptor, but its active Zn(II) complex is effective and supports chelation-enhanced biological activity. This led to a significant decrease in the binding energy of the coordination. The activity of Zn(II) complex was found to be better than that of HL, indicating that zinc complex may serve as a better future anti-gastroenteritis therapeutic agent.

Journal of Chemical Health Risks
www.jchr.org
JCHR (2025) 15(4), 391-408 | ISSN:2251-6727

TABLE 9: Computed Interaction Energy Values: Docking Analysis of Schiff Base Ligand **(HL)** with Varied Protein Receptors Associated with *H. Pylori,*

Cancer Cells, and COVID-19

type	Receptor	Ligand moiety	Receptor site	Interaction	Distance (A^0)	E (kcal/mol)
	2JFZ	No activity	No activity	No activity	No activity	No activity
Cancer cells	**1SC7**	N 4	O CYS 630 (A)	H-donor	3.15	-1.5
		N 10	O ASN 631 (A)	H-donor	3.03	-1.4
		6-ring	ND2 ASN 631 (A)	pi-H	3.79	-2.5
COVID 19	**6W41**	6-ring	OH TYR 176 (H)	pi-H	3.92	-0.7

TABLE 10: Energy of Interaction Results from Docking Calculations of Zinc (II) complex with Various Protein Receptors Associated with *H. pylori*, Cancer Cells, and COVID-19.

type	Receptor	Ligand moiety	Receptor site	Interaction	Distance (A^0)	E (kcal/mol)
H. Pylori	**2JFZ**	O 20	6-ring TRP 252 (A)	cation-pi	4.50	-1.5
		O 20	5-ring TRP 252 (A)	cation-pi	4.11	-4.4
		6-ring	CZ2 TRP 244 (A)	pi-H	4.50	-0.7
Cancer cells	**1SC7**	N 4	O2P PTR 723 (A)	H-donor	3.03	-7.6
		N 10	O2P PTR 723 (A)	H-donor	3.14	-3.9
		N 10	O3P PTR 723 (A)	H-donor	3.44	-0.8
		O 22	O2P PTR 723 (A)	H-donor	2.97	-17.4
		O 22	O3P PTR 723 (A)	H-donor	2.89	-1.3
		O 22	O2P PTR 723 (A)	ionic	2.97	-4.7
		6-ring	NZ LYS 587 (A)	pi-cation	4.75	-1.7
		6-ring	CB ASN 722 (A)	pi-H	4.48	-1.0
		O 20	OE2 GLU 148 (H)	H-donor	3.33	-3.2
COVID 19	**6W41**	O 22	OE2 GLU 148 (H)	H-donor	2.58	-12.7
		O 20	OE2 GLU 148 (H)	ionic	3.33	-2.6
		O 22	OE2 GLU 148 (H)	ionic	2.58	-8.0

TABLE 11: Molecular docking 2D and 3D for predicting the possible binding modes of the studied (HL) and its Zinc (II) complex, with the receptors of the crystal structure from Protein Data Bank of different types of receptors (2JFZ , 1SC7 and 6W41).

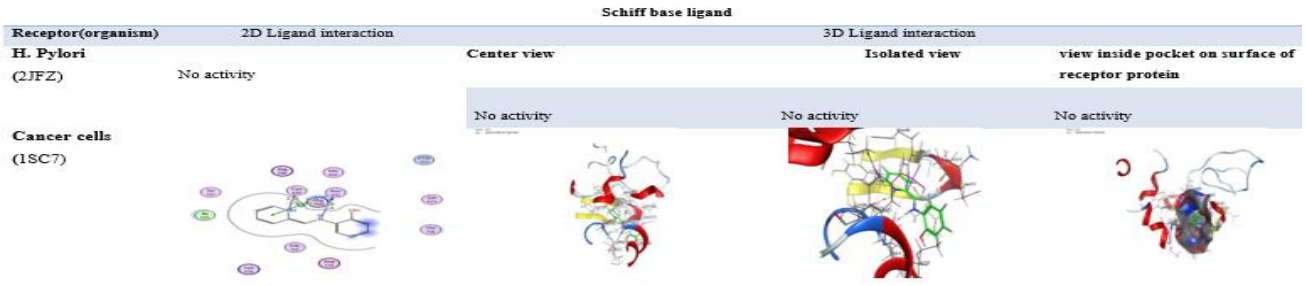

Journal of Chemical Health Risks
www.jchr.org
JCHR (2025) 15(4), 391-408 | ISSN:2251-6727

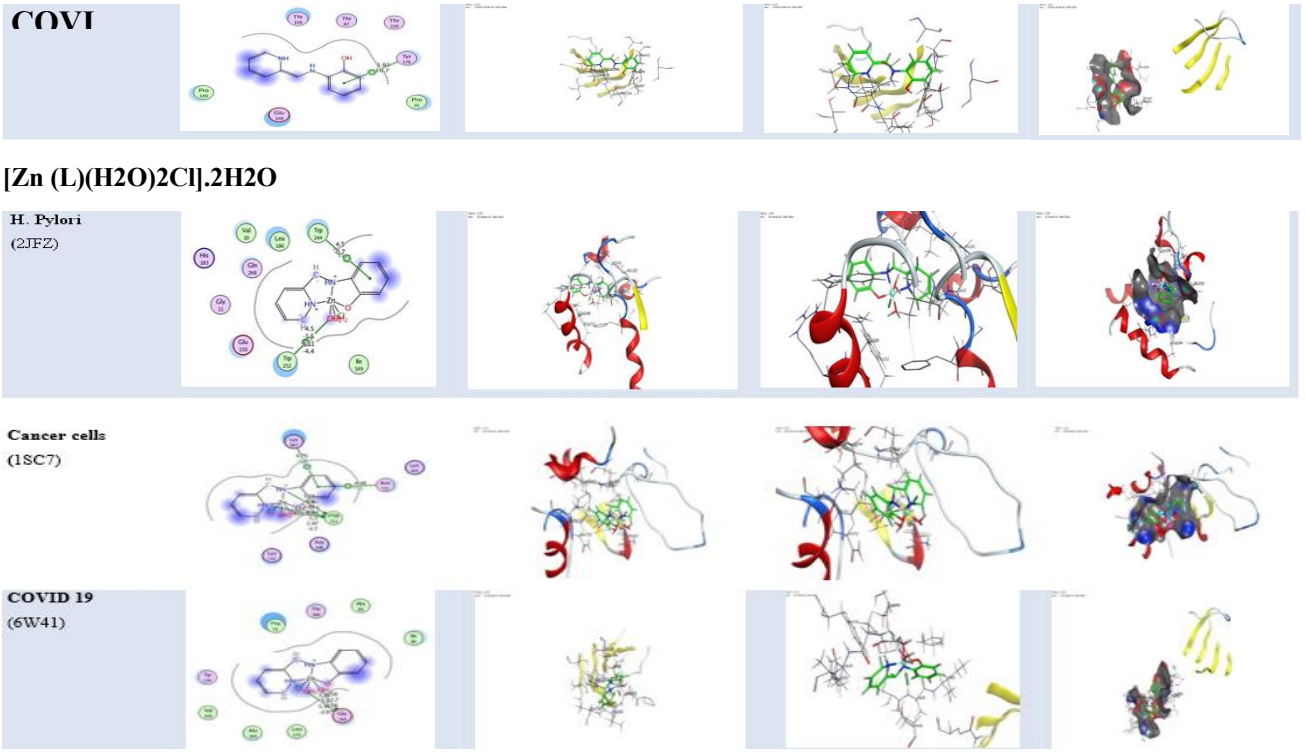

Conclusion

This work describes the characterization of a tridentate Schiff base ligand (HL) and several metal complexes by elemental analysis, molar conductance, mass spectrometry, 1H-NMR, magnetic susceptibility and IR and UV-visible spectroscopy. The analyses clarified the features of octahedral type complexes. These compounds exhibited broad-spectrum antimicrobial activities and strong anticancer activities against MCF-7 cells. Notably, these complexes showed a low cytotoxic effect on normal VERO cells compared to the established chemotherapeutic cisplatin, rendering them suitable for prospective therapeutic usage. Finally, the results from the computational (DFT) and molecular docking studies show that these compounds may also have the potential to inhibit some of the H. Pylori, tumors, and the coronavirus (which causes COVID-19) protein targets. In summary, this study indicates a new pathway towards the next multi-target agent that could be safer and more efficacious in the management of microbial diseases and cancer.

References

1- B. F. Perry, A. E. Beezer, R. J. Miles, B. W. Smith, J. Miller and M. G. Nascimento, Microbois., 1988, 45,181.
2- A. Elmali, M. Kabak and Y. Elerman, J. Mol. Struct., 2000, 477, 151.
3- P. R. Patel, B. T. Thaker and S. Zele, Indian J. Chem., 1999, 38 A, 563.
4- M. Valcarcel and M. D. Laque de Castro, "Flow-Throgh Biochemical Sensors", Elsevier, 1994, Amsterdam.
5- U. Spichiger-Keller, "Chemical Sesors and Biosensors for Medical and Biological Applications", Wiley-VCH, 1998, Weinheim.
6- J. F. Lawrence and R. W. Frei, "Chemical Derivatization in Chromatography", Elsevier, 1976, Amsterdam.
7- S. Patai, Ed., "The Chemistry of the Carbon-Nitrogen Double Bond", J. Wiley & Sons, 1970, London.
8- P. Singh, R. L. Goel and B. P. Singh, J. Indian Chem. Soc., 1975, 52, 958.
9- S. D. Ittel, L. K. Johnson, M. Brookhart, Chem. Rev., 2000, 100, 1169.
10- J.J.Bao, Meny and Rintoul, Coordination Chemistry Reviews, 2006, 250 (3-4), 424-448.
11- H. Nora. Al-Shaalan, Molecules, 12, 1080-1091 (2005).
12- L. Savanini, L. Chiasserini, A. Gaeta, C. Pellerano, Biorg. Med. Chem. 2007, 10, 2193-2198.
13- R. K. Agarwal, L. Singh, D.K Sharma, Turk J.Chem, 2007, 29, 309 – 310.
14- G. H. Olie, and S. Olive, Springer, Berlin (1984).
15- S. Li, S. Chen, H.Ma, R. Yu and D. Liu, Corros. Sci, 1999, 41, 1273.
16- Accelrys Software Inc, Discovery Insight, Accelrys Software Inc, San Diego, CA, USA, 2009.
17- National Committee for Clinical Laboratory Standards. Method for Antifungal Disc Diffusion Susceptibility Testing of Yeast: Proposed Guideline M44-P. Wayne, PA, USA (2003).
18- WH.Mahmoud, GG. Mohamed, MMI. El-Dessouky, Coordination modes of bidentate lornoxicam drug with some transition metal ions. Synthesis, characterization

and in vitro antimicrobial and antibreastic cancer activity studies, Spectrochim.Acta AJ.Mol. Biomol. Spectrosc. 2014,122:598–608.

19- I. Sakıyan, E. Logoglu, S. Arslan, N. N.Sari, S ¸ N. akıyan, Antimicrobial activities of N-(2-hydroxy-1-naphthalidene)-amino acid(glycine, alanine, phenylalanine, histidine, tryptophane) Schiff bases and their manganese(III) complexes, Biometals. 2004,17:115–120.

20- P. Skehan, R. Storeng, D. Scudiero, A. Monks, J. McMahon, D. Vistica, JT. Warren, H. Bokesch, S. Kenney, MR. Boyd, New colorimetric cytotoxicity assay for anticancer-drug screening, J. Natl. Cancer Inst. 1990,42:1107–1112.

21- C. Balakrishnan, L. Subha, M. A. Neelakantan, S. S. Mariappan, Spectrochim. Acta A. 2015, 150, 671.

22- S.Sangilipandi, D.Sutradhar, K.Bhattacharjee, W.Kaminsky, SR. Joshi , AK. Chandra, KM. Rao, Inorg. Chim. Acta. 2016;441:95. CJ. Dhanaraj, IU. Hassan, J. Johnson, J. Joseph, RS. Joseyphus, J. Photochem. & B. Photobio: Bio. 2016,162:115.

23- S.M. Pradeepa, H.S.B. Naik, B.V. Kumar, K.I. Priyadarsini, A. Barik, M.C. Prabhakara, DNA binding, photoactivated DNA cleavage and cytotoxic activity of Cu (II) and Co (II) based Schiff-base azo photosensitizers. Spectrochim. Acta A, 2015,141, 34–42.

24- E.M. Zayed, E.H. Ismail, G.G. Mohamed, M.M.H. Khalil, A.B. Kamel, Synthesis, spectroscopic and structural characterization, and antimicrobial studies of metal complexes of a new hexadentate Schiff base ligand. Spectrophotometric determination of Fe (III) in water samples using a recovery test. Monatsh. Chem. 2014, 145, 755–765.

25- B. Hammer, L. B. Hansen, and J. K. Nørskov, “Improved adsorption energetics within density-functional theory using revised Perdew-Burke-Ernzerhof functionals,” Physical Review B, vol. 59, no. 11, p. 7413, 1999.

26- A. Matveev, M. Staufer, M. Mayer, and N. R¨osch, “Density functional study of small molecules and transition-metal carbonyls using revised PBE functionals,” International Journal of Quantum Chemistry, vol. 75, no. 4-5, pp. 863–873, 1999.

27- M. Hanif, Z.H. Chohan, Spectrochim. Acta A, 2013, 104, 468–476.

28- A.M.A. Alaghaz, H.A. Bayoumi, Y.A. Ammar, S.A. Aldhlmani, J. Mol. Str. ,2013,1035, 383–399,

29- S.Ilhan, Russ. J.Coord.chem. 2009,35(5),347-351.

30- 27- M.Anu*, P.Lakshmi Prabha, G.Banukarthi, P.Rexy Kanjana, K.Rajeshwari“UV-VISIBLE, IR AND NMR SPECTRA ON COPPER (II) SCHIFF BASE COMPLEX ” International Standard Serial Number (ISSN): 2249-6807 International Journal of Institutional Pharmacy and Life Sciences 3(6) , 23 - 32: November-December 2013

31- G.G. Mohamed, M.M. Omar, A.A. Ibrahim, Eur. J. Med. Chem.; 2009,44: 4801-4812.

32- V.LDorofeev, Pharm. Chem, J; 2004, 38: 45-49.

33- M.S. Refat, G.G. Mohamed, R.F. Farias, A.K. Powell, M.S. El-Garib, S.A. El-Korashy, M.A. Hussien, J. Therm. Anal. Calor., 2010, 102: 225–232.

34- M.S. Refat, G. G.Mohamed, J. Chem. Eng. Data, 2010, 55: 3239–3246.

35- L.J. Bellamy, The Infrared Spectra of Complex Molecules, third ed., Chapman and Hall, London, , 1975.

36- K.D. Patel, H.S. Patel, Arab. J. Chem., 2013, article in press.

37- Anu, M., Prabha, L., Banukarthi, G., Kanjana, P. R., & Rajeswari, K. (2013). UV-visible, IR and NMR spectra on Copper (II) Schiff base Complex. International Journal of Institutional Pharmacy and Life Sciences, 3(6), 23–32.

38- W.H.Mahmoud,G.G. Mohamed,M.M.I. El-Dessouky, Spectrochim Acta A.2014,122,598-608.

39- Acta Chim. Pharm. Indica: 3(2), 2013, 127-134 ISSN 2277-288X (COORDINATION BEHAVIOR OF N/O DONOR LIGAND WITH SOMETRANSITION METALSMUNA ABASS HADI

40- Y.T. Liu, G.D. Lian, D.W. Yin, B.J. Su, Spectrochim. Acta A.2013,100, 131–137.

41- W.H. Mahmoud,N.F.Mahmoud,G.G.Mohamed,A.A.El-Bindary,A.Z. El-Sonbati,J.Mol.str.2015,1086,266-275.

42- Lever ABP. Inorganic electronic spectroscopy;,2nd ed. NewYork: Elsevier,1997.

43- A.M.A. Alaghaz, H.A. Bayoumi, Y.A. Ammar, S.A. Aldhlmani, J. Mol. Str. 2013,1035, 383–399.

44- FA. Cotton, G .Wilkinson, CA .Murillo, M. Bochmann, Advanced inorganic chemistry.;6th ed. New York: Wiley. 1999,

45- G.G. Mohamed, E.M.Zayed,A.M.M. Hindy,spectrochim.Acta A. 2015,145,76-84

46- AD .McLean, GS. Chandler, Contracted Gaussian-basis sets for molecular calculations. 1. 2nd row atoms, Z = 11–18. J Chem Phys. 1980;72:5639–48.

47- TH Jr Dunning, PJ. Hay, In: Schaefer III HF, editor. Modern theoretical chemistry, vol 3. New York: Plenum; 1977. p. 1–28.

48- Y .Prashanthi, K .Kiranmai, NJP .Subhashini, S. Shivaraj .Synthesis, potentiometric and antimicrobial studies on metal complexes of isoxazole Schiff bases. Spectrochim Acta A. 2008;70:30–5.

49- EM .Zayed, E.H. Ismail, G.G. Mohamed, M.M.H. Khalil.A.B. Kamel, Monatsh. Fur Chem. 2014,145(5),755-765.

50- P.Tyagi, S. Chandra, B.S. Saraswat, D. Yadav , Spectrochim. Acta A. 2015, 145, 155-164.

51- Schlegel, H. B. (1982). Optimization of equilibrium geometries and transition structures. Journal of Computational Chemistry, 3(2), 214–218.

52- Tyagi, P., Tyagi, M., Agrawal, S., Chandra, S., Ojha, H., & Pathak, M. (2017). Synthesis, characterization of 1, 2, 4-triazole Schiff base derived 3d-metal complexes: Induces cytotoxicity in HepG2, MCF-7 cell line, BSA binding fluorescence and DFT study. Spectrochimica Acta Part A: Molecular and Biomolecular Spectroscopy, 171, 246–257.

53- Abdou, A.; Hassan, M.M.; Abdel-Mawgoud, M. Seven metal-based bi-dentate NO azocoumarine complexes: Synthesis, physicochemical properties, DFT calculations, drug-likeness, in vitro antimicrobial screening and molecular docking analysis. Inorg. Chim. Acta 2022, 539, 121043.

54- Ali El-Remaily, M.A.E.A.A.; El-Dabea, T.; Alsawat, M.; Mahmoud, M.H.; Alfi, A.A.; El-Metwaly, N.; Abu-Dief, A.M. Development of new thiazole complexes as powerful catalysts for synthesis of pyrazole-4-carbonitrile derivatives under ultrasonic irradiation condition supported by DFT studies. ACS Omega 2021, 6, 21071–21086.

55- Joseyphus, R. S., & Nair, M. S. (2008). Antibacterial and antifungal studies on some schiff base complexes of zinc (II). Mycobiology, 36(2), 93–98.

56- Mahmoud, W. H., Deghadi, R. G., & Mohamed, G. G. (2017). Preparation, geometric structure, molecular docking thermal and spectroscopic characterization of novel Schiff base ligand and its metal chelates: Screening their anticancer and antimicrobial activities. Journal of Thermal Analysis and Calorimetry, 127, 2149–2171.

57- Neelakantan, M. A., Marriappan, S. S., Dharmaraja, J., Jeyakumar, T., & Muthukumaran, K. (2008). Spectral, XRD, SEM and biological activities of transition metal complexes of polydentate ligands containing thiazole moiety. Spectrochimica Acta Part A: Molecular and Biomolecular Spectroscopy, 71(2), 628–635.

58- Mahmoud, W. H., Sayed, F. N., & Mohamed, G. G. (2016). Synthesis, characterization and in vitro antimicrobial and anti-breast cancer activity studies of metal complexes of novel pentadentate azo dye ligand. Applied Organometallic Chemistry, 30(11), 959–973.

59- H. F. Abd El-Halim, M. M. Omar, G. G. Mohamed, Spectrochim. Acta A 2011, 78, 36–44.

60- H. F. Abd El-Halim, G. G. Mohamed, J. Mol. Struct. 2016, 1104, 91–5.

61- W. H. Mahmoud, N. F. Mahmoud, G. G. Mohamed, A. A. El-Bindary, A. Z. El-Sonbati,J.Mol.Struct.2015,1086,266–75.

62- Zafar, H., Kareem, A., Sherwani, A., Mohammad, O., Ansari, M. A., Khan, H. M., & Khan, T. A. (2015). Synthesis and characterization of Schiff base octaazamacrocyclic complexes and their biological studies. Journal of Photochemistry and Photobiology B: Biology, 142, 8–19.

63- Khan, T. A., Naseem, S., Hajra, R., & Shakir, M. (2010). Synthesis, Physicochemical, and Antimicrobial Screening Studies of Complexes of Co (II), Ni (II), Cu (II), and Zn (II) with 18-membered Schiff Base Octaazamacrocyclic Ligand. Synthesis and Reactivity in Inorganic, Metal-Organic, and Nano-Metal Chemistry, 40(10), 861–868.

64- Cotton, F. A., Wilkinson, G., Murillo, C. A., & Bochmann, M. (1999). Advanced inorganic chemistry. John Wiley & Sons.

65- El-Boraey, H. A., & El-Din, A. A. S. (2014). Transition metal complexes of a new 15-membered [N5] penta-azamacrocyclic ligand with their spectral and anticancer studies. Spectrochimica Acta Part A: Molecular and Biomolecular Spectroscopy, 132, 663–671.

66- Mosmann, T. (1983). Rapid colorimetric assay for cellular growth and survival: application to proliferation and cytotoxicity assays. Journal of Immunological Methods, 65(1–2), 55–63.

67- Shah, R., Alharbi, A., Hameed, A. M., Saad, F., Zaky, R., Khedr, A. M., & El-Metwaly, N. (2020). Synthesis and structural elucidation for new Schiff base complexes; conductance, conformational, MOE-docking and biological studies. Journal of Inorganic and Organometallic Polymers and Materials, 30, 3595–3607.

68- B. Delley, “A scattering theoretic approach to scalar relativistic corrections on bonding,” International Journal of Quantum Chemistry, vol. 69, no. 3, pp. 423–433, 1998.

69- B. Delley, “From molecules to solids with the DMol3 approach,” 0e Journal of Chemical Physics, vol. 113, no. 18, pp. 7756–7764, 2000.

70- A. Kessi and B. Delley, “Density functional crystal vs. cluster models as applied to zeolites,” International Journal of Quantum Chemistry, vol. 68, no. 2, pp. 135–144, 1998.

71- W. J. Hehre, L. Radom, P. v. R. Schleyer, and J. A. Pople, Ab Initio Molecular Orbital 0eory, Wiley, New York, NY, USA, 1986.